Large eddy simulation of flow around the Ahmed body

C. Hinterberger, M. García-Villalba, and W. Rodi

Institute for Hydromechanics, University of Karlsruhe, Kaiserstrasse 12, 76128 Karlsruhe, Germany

1 Introduction

The automotive industry has a high demand for reliable simulation methods capable of tackling the complex turbulent air flow around vehicles. The Ahmed reference model is a generic car-type bluff body with a slant back. It is frequently used as a benchmark test case for this kind of flow. In spite of the relatively simple geometry of the Ahmed body, the flow around it retains some main features of the flow around real cars.

The Ahmed body, Fig. 1, was first defined and its characteristics described in the experimental work of Ahmed et al [1]. Therein, it is shown that most of the drag of the body is due to pressure drag, which is generated at the rear end. The structure of the wake is very complex, with a separation zone and counter-rotating vortices coming off the slant side edges, whose strength is mainly determined by the base slant angle. The maximum drag was found for a critical slant angle of $30\,^\circ$. Above this angle a sudden drop in drag occurs which corresponds to a change in the wake structure. Below this angle, strong counter-rotating vortices are present and the flow separates in the middle region of the top edge and reattaches at the sloping surface. For angles above the critical angle, the counter-rotating vortices are weaker, the separation occurs along the entire top and the side edges and there is no reattachment.

More recently, Lienhart et al [2] performed more detailed experiments on the same body, albeit at a somewhat lower velocity. They measured the mean and fluctuating velocities by LDA and obtained surface oil-flow pictures for two rear vehicle body slant angles ($\varphi = 25\,^\circ$ and $\varphi = 35\,^\circ$), i.e. just below and above the critical angle. Their results show the differences in flow behaviour for the two angles considered.

In recent years, there have been several computational studies of this flow. Han [3] and Gilliéron and Chometon [4] using the RANS approach obtained qualitatively good results in terms of flow structures but they do not show velocity profile comparisons. In two recent workshops [5, 6] the flow around the Ahmed body was a test case and the results presented there have shown

that it is difficult with classical RANS methods to obtain accurate predictions of mean velocitiy and turbulence intensitiy profiles for this flow. With other approaches the results have been similar, for example, Kapadia et al [7] using DES (Detached Eddy Simulation). Finally, there is a Large Eddy Simulation reported in the literature, [8], however the flow conditions were different (no ground was present) so that these results are not directly comparable with the experiments.

In this paper we present two Large Eddy Simulations of the first configuration ($25°$) of the experiment of Lienhart et al [2], while the work for the second configuration ($35°$) is in progress.

The outline of the paper is as follows. In section 2 the simulation details will be presented, the computational setup will be discussed and the grids will be described. In section 3.1, some quantitave results will be presented, in terms of mean velocity and turbulent intensity profiles. Flow visualisation and turbulent coherent structures will be discussed in section 3.2. Finally, some conclusions will be made in section 4.
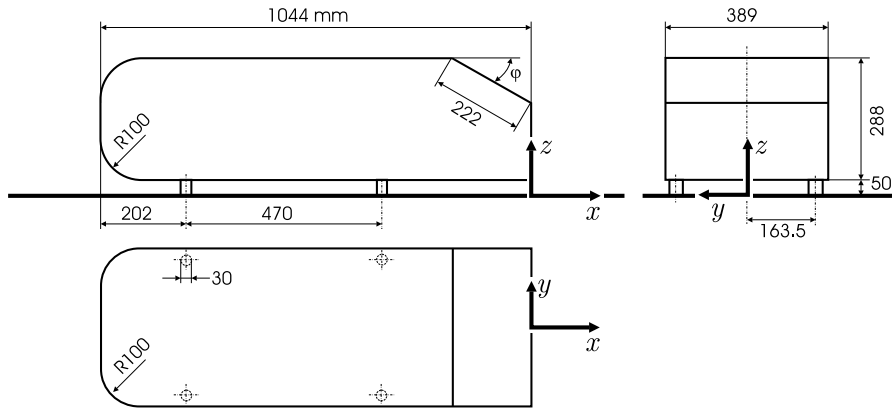
Fig. 1. Ahmed model. Dimensions are in mm

2 The simulated configuration

The present configuration has been specifically chosen to match the experiment of Lienhart et al [2]. The Ahmed body, whose shape and dimensions are shown in Fig. 1, was mounted in a 3/4 open test section (floor, but no side walls or ceiling). The bulk velocity was 40 m/s. This results in a Reynolds number $Re = 2.8 \times 10^6$ (based on the length of the body $L = 1.044$ m), which is of the same order of magnitude but somewhat lower as the one in the original experiment of Ahmed et al [1] ($Re = 4.3 \times 10^6$).

2.1 Numerical method

The simulations were performed with the Finite Volume Code LESOCC$_2$ (Large Eddy Simulation On Curvilinear Coordinates) which is an enhanced fully-parallelized version of the code LESOCC [9], developed at the Institute for Hydromechanics. It solves the incompressible 3D time-dependent filtered Navier-Stokes equations on body-fitted curvilinear block-structured grids using second order central differences for the discretisation of the convective and viscous fluxes. Time advancement is accomplished by an explicit, low-storage Runge-Kutta method. Conservation of mass is achieved by the SIMPLE algorithm, with the pressure-correction equation being solved by the SIP procedure. The momentum-interpolation method of Rhie and Chow [10] is employed to prevent pressure-velocity decoupling and associated oscillations.

2.2 Computational setup

The flow around the Ahmed body was a test case in two recent workshops [5, 6], the computational domain was defined in them. The domain extends to five body lengths behind the body to ensure that the outflow condition does not affect the near-body wake. The inflow plane is placed at a distance of 1.3 body lengths upstream of the body. This distance corresponds roughly to 5 body heights where blocking effects dissapear. At the inflow section a uniform axial velocity profile is imposed. The width of 1.87 m (5 body widths) and the height of 1.4 m (5 body heights) are taken analogous to the experiments. At both side boundaries and at the top boundary, free-slip conditions are applied. At the outflow of the domain, a convective boundary condition for the velocities is used. Finally, wall functions are used because of the high Reynolds number which does not allow a fine resolution of the near wall flow down to the viscous sub-layer. The wall function is similar to the Werner-Wengle [11] approach but assuming an instantaneous logarithmic profile instead of a power law profile. It is applied at the walls of the vehicle and at the bottom of the channel. In order to account for the unresolved subgrid-scale motions, the Smagorinsky subgrid-scale model is employed with a model constant of $C_s = 0.13$.

2.3 Grids

In this paper we present simulations of the flow around the 25° slant-back Ahmed body performed with two grids. They have been generated with the commercial software ICEM-CFD. Grid 1 consist of 93 blocks and 8.8 10^6 cells. Grid 2 consist of 214 blocks and 18.5 10^6 cells. Both grids have an O-grid structure around the body, which is necessary due to the round body front. This allows for grid refinement in the wall-normal direction near the body boundaries. The outer block structure of Grid 1 is orthogonal, Fig 2(a). In order to get a concentration of grid points close to the body in spanwise

and streamwise direction, an outer O-grid structure was chosen in Grid2, Fig 2(b). In addition, Grid 2 includes more refinement in the region of the slant back, especially close to the top and side edges, Fig 2(c-h). For both grids, the near-wall cell centre has a wall distance on average of about 40 wall units (Δy_P^+), but it varies from approximately 10 in the separated regions along the slant back to 150 close to the top rear edge. The spanwise and streamwise extent of the grid cells is up to a factor of 10 larger for Grid 2, except in the refinement regions close to the edges. For Grid 1 this factor is even larger. This means that the boundary layer at the body surface is highly underresolved.
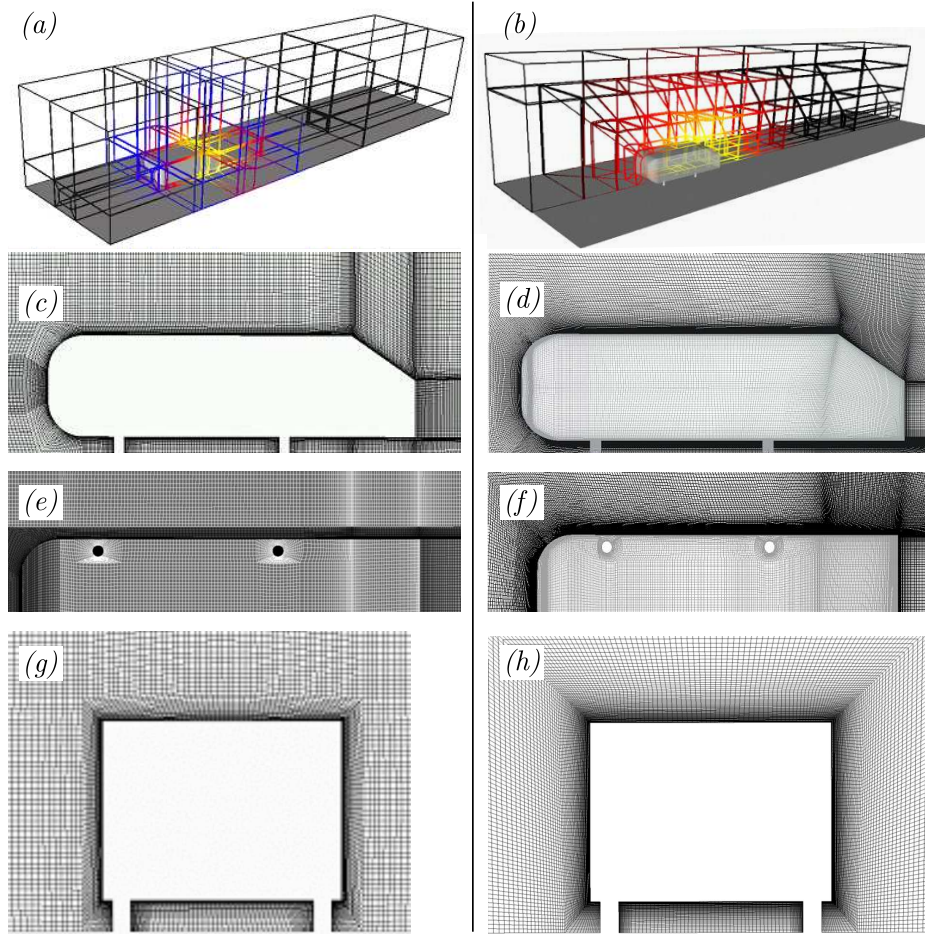
Fig. 2. Typical grids used for the LES. *(a,c,e,g)* Grid 1. *(b,d,f,h)* Grid 2. *(a,b)* Sketches of the block structure. *(c-h)* Slices in different planes showing the grid point distribution in the body region. *(c,d)* Cut in xz-plane . *(e,f)* Cut in xy-plane. *(g,h)* Cut in yz-plane.

3 Results

3.1 Time averaged profiles

For the front part, mean streamwise velocity profiles in the symmetry plane are compared with the experiment in Fig. 3. It can be seen that the flow upstream of the body and in the free stream above it is properly represented in the simulation. This is because in this region the level of turbulence is so low that the flow is nearly potential flow.
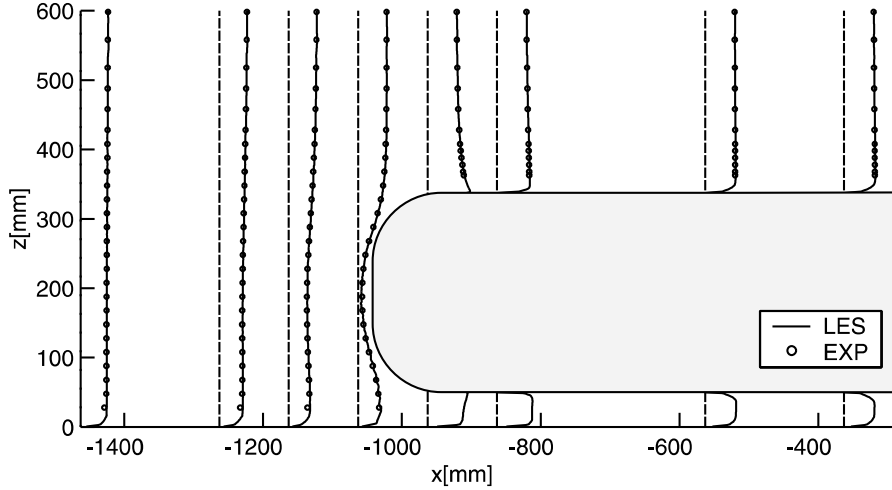
Fig. 3. Mean streamwise velocity profiles in the symmetry plane

In Figures 4 and 5, the mean streamwise velocity profiles and root mean square velocity fluctuations are compared with the experimental results in the rear body part and the near wake (in the symmetry plane). The general agreement with the experiment is reasonably good taking into account that neither grid is fine enough to resolve adequately the boundary layer developing on the body up to the slant back. However there are some discrepancies between the computations and the experiment mainly concerning the velocity profiles on the slant back. In the experiment, the flow separates right at the corner of the sloping surface and it reattaches in the middle of the surface. In the simulation, the flow first stays attached before it separates somewhat downstream of the corner and no reattachment occurs on the slant back. This is most likely due to the poor resolution of both grids near the wall leading to an incorrect prediction of the approaching boundary layer.

The main differences between the results of the two simulations are found at the beginning of the sloping surface. There, Grid 2 is much finer than Grid 1, and it can be seen that the turbulence intensities are very close to the
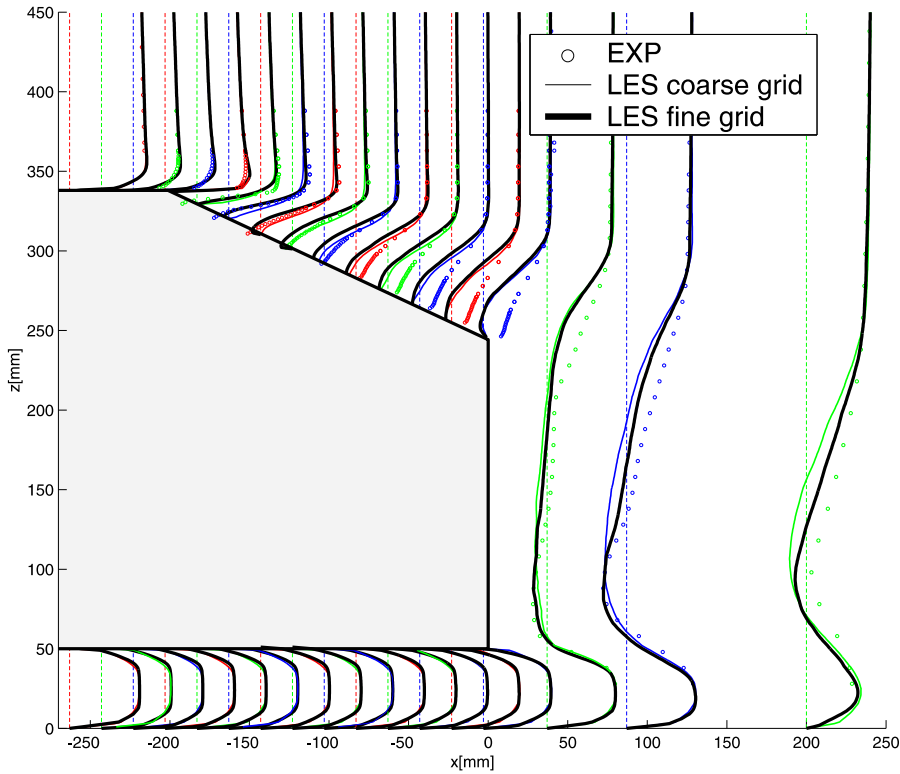
Fig. 4. Mean streamwise velocity profiles in the rear body and near wake (symmetry plane)

experimental ones for Grid 2 while they are too low for Grid 1, Fig. 5. In addition, the prediction of the separation point is closer to the experiment in the simulation performed with the finer grid, in which the flow separates earlier, Fig. 4.

The complex unsteady flow on the slant back leads to high fluctuation intensities which are very difficult to predict. In fact, no RANS method has succeeded in predicting the high values observed in the experiments [5, 6] while the present LES calculations (Fig. 5) have.

Figure 6 shows the mean velocity vectors in the symmetry plane, Fig. 6(a-b), and in three transverse yz-planes, Fig. 6(c-h). The streamwise location of these transverse planes is indicated in Fig. 6(a) by dashed lines. The colour of the vectors corresponds to turbulent kinetic energy. From the comparison of the experiment, Figs. 6(a,c,e,g) on the left, with the simulation, Figs. 6(b,d,f,h) on the right, it is clear that the main flow structures are well captured in the simulation. The size and the extent of the recirculation zone behind the body are well predicted, Fig. 6(b). The development of the counter-rotating vortices, which can be seen from the secondary flow vectors in the
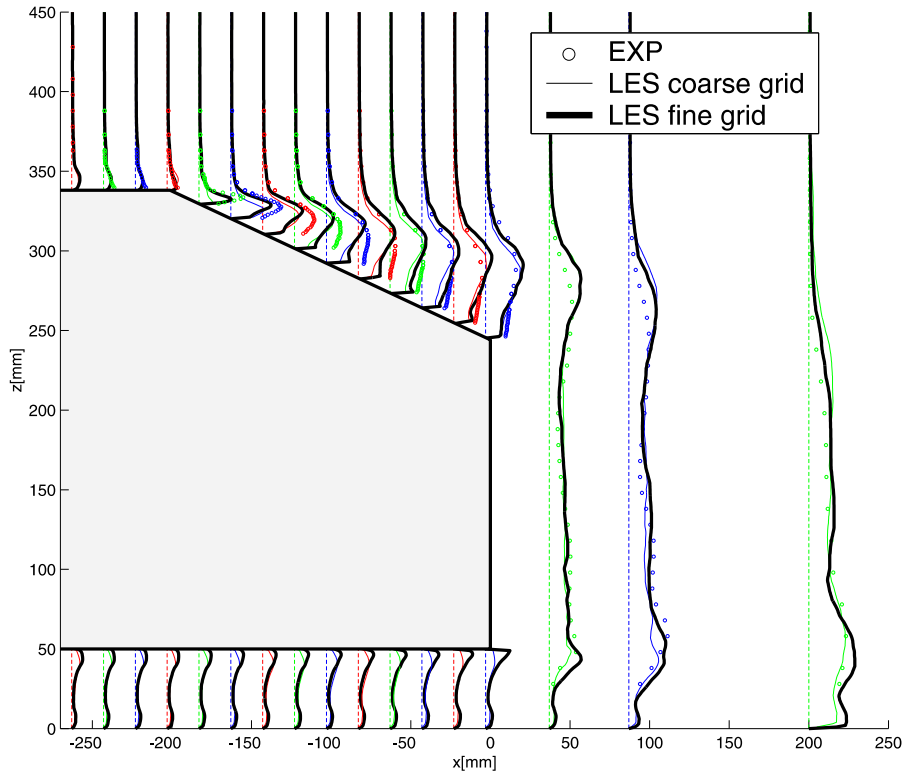
Fig. 5. Root mean square streamwise velocity fluctuations in the rear body and near wake (symmetry plane)

$y-z$ planes, is also in close agreement with the experiment. In Fig. 6 *(d)*, it can be seen that these vortices develope half-way down the slant back, they grow while they approach the end of the body, Fig. 6 *(f)*, and they are strong and fully developed in the near wake, Fig. 6 *(h)*. The level of turbulence obtained in the simulation is also in good agreement with the experiment, as can be seen from the coloured regions in Figure 6.

3.2 Flow visualisation and flow structures

The calculation results show complex time-dependent flow features in the wake region. In Fig. 7, two typical instantaneous velocity fields in the symmetry plane are shown. As discussed in section 3.1, the prediction of the flow on the sloping surface is very difficult. Thus, in Fig. 7 on the left, an instantaneous field is captured in which the flow tends to reattach on the slant back. However, in Fig. 7 on the right, the flow in that zone is completely separated. Note that in the experiment the flow reattaches (at least in the mean). The unsteadiness of the near body-wake is clearly well captured. The flow between the body and
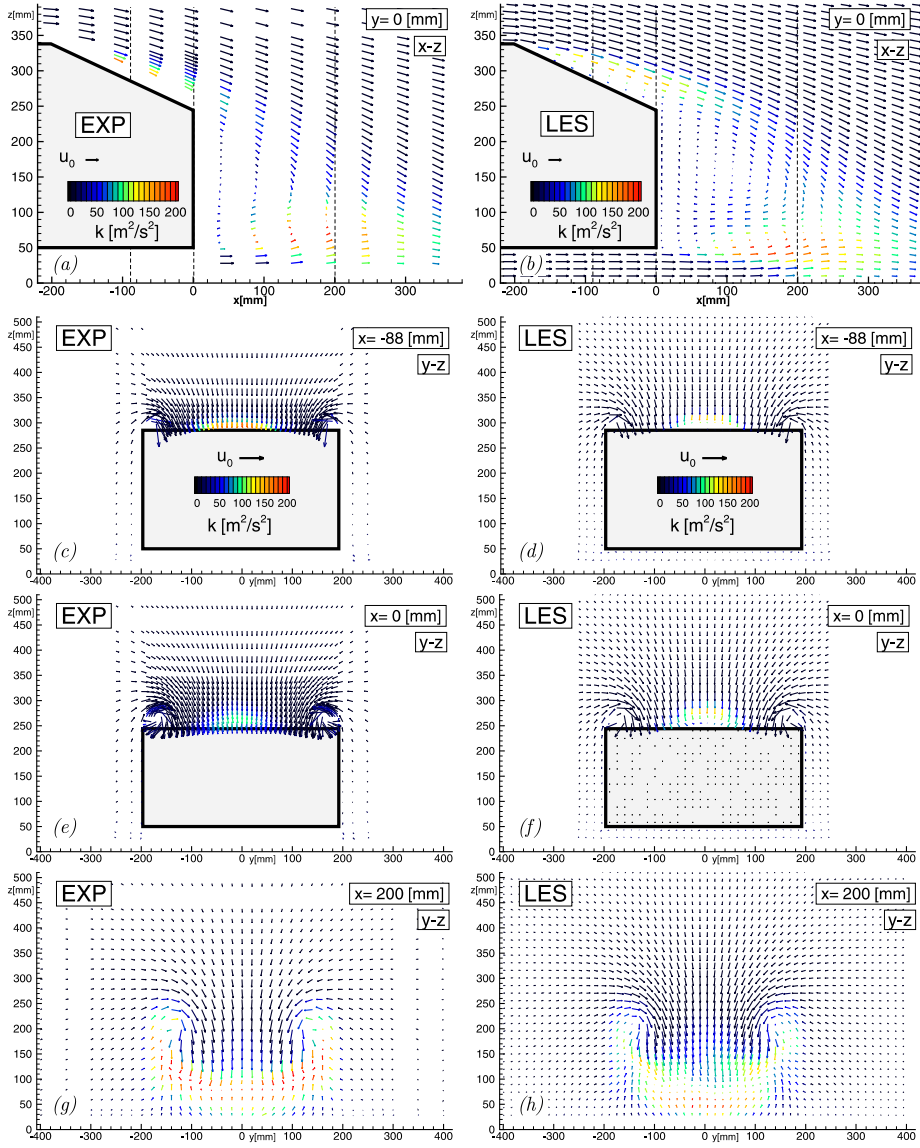
Fig. 6. Mean velocity vectors coloured by turbulent kinetic energy. *(a,b)* symmetry plane $y = 0$ mm. *(c,d)* Close to the middle of the slant back $x = -88$ mm. *(e,f)* End of the body $x = 0$ mm. *(g,h)* Near-body wake $x = 200$ mm. *(a,c,e,g)* Experiment. *(b,d,f,h)* Simulation performed with Grid 2.

the ground plate has a rather strong influence on the shape of the recirculation zone.
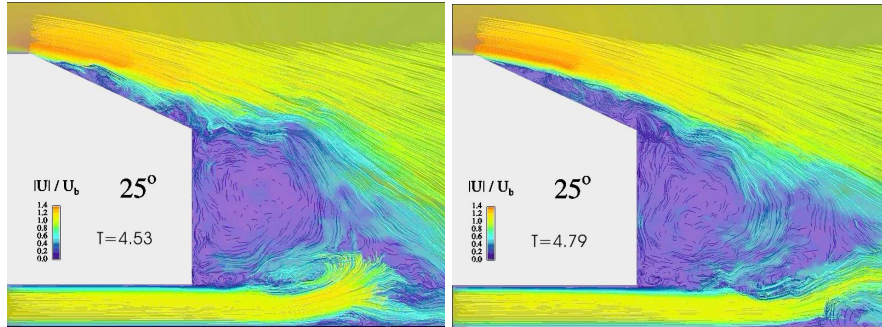
Fig. 7. Instantaneous streamwise velocity fields in the symmetry plane

In order to illustrate the presence of large-scale vortices in the recirculation zone, Fig. 8 shows the isosurfaces of pressure fluctuations p' for three sequential instants in time. The main part gives a perspective view while the three pictures on the left give the side view, top view and view from the back respectively. It can be seen that large spanwise vortex tubes are generated near the leading edge of the slanted face, which grow and roll down the surface. Furthermore, vortex tubes that wrap the counter-rotating vortices coming off the slant side edges can be detected. The sequential pictures show that these vortex tubes form helical structures as they move downstream.

3.3 Work in progress

Preliminary simulations have been performed for the second case ($\varphi = 35°$) of the experiment of Lienhart et al [2]. The first results are not very satisfactory. In that case, the flow separates along the top and side edges and the counter-rotating vortices are weaker. In the preliminary simulations, this behaviour is not well captured. Furthermore, the drag coefficient for this case is not well-predicted. The experiment of Ahmed et al [1] has shown that above a slant back angle of 30°, there is a drop in the drag coefficient. While in the simulation for the 25° case the prediction of the drag was good, in the preliminary simulations for the 35° case, the drop in the drag does not take place, and the drag coefficient is highly over-predicted. This may be due to the poor resolution of the near wall regions but further investigation is required.

4 Conclusions

A Large Eddy Simulation of the flow around the Ahmed body with a slant-back angle of 25° was performed. The flow around the Ahmed body is a very
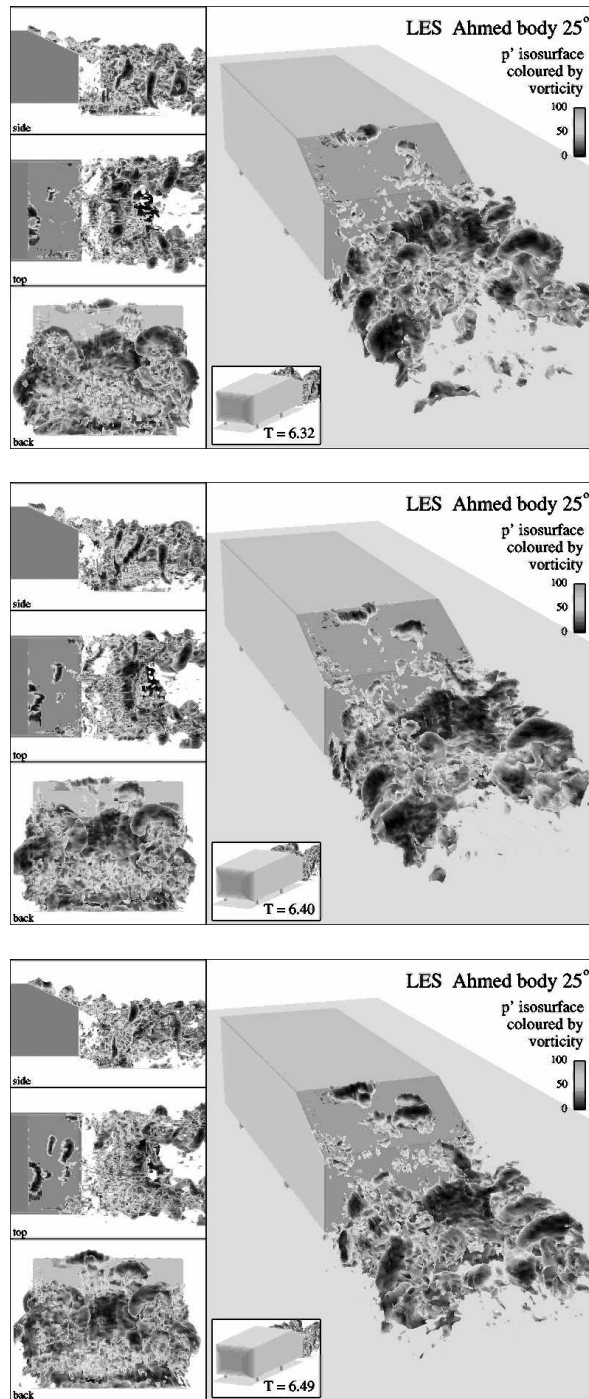
Fig. 8. Isosurface of pressure fluctuations

challenging problem because of the complex geometry and the high Reynolds number. The results obtained by the simulation are promising; the comparison with the experiments shows that the flow structures are well captured. The agreement of the time-averaged quantities is good although some discrepancies are present, especially in the lower part of the slant back. The results also show that this is a good test case for further development. The calculations for the configuration with a slant angle of 35 ° are in progress. Improvements of the method (subgrid-scale model, discretisation, wall modelling, etc) are required to obtain good results for the 35 ° case.

Acknowledgments

References

1. S.R. Ahmed, G. Ramm, and G. Faltin. Some salient features of the time averaged ground vehicle wake. SAE paper no. 840300, 1984.
2. H. Lienhart, C. Stoots, and S. Becker. Flow and turbulence structures in the wake of a simplified car model (Ahmed model). In *DGLR Fach Symp. der AG STAB*, 2000.
3. T. Han. Computational analysis of three-dimensional turbulent flow around a bluff body in ground proximity. *AIAA Journal*, 27:1213–1219, 1989.
4. P. Gilliéron and F. Chometon. Modelling of stationary three-dimensional separated air flows around an Ahmed reference model. In *ESAIM proc.*, volume 7, pages 173–182, 1999.
5. S. Jakirlić, R. Jester-Zürker, and C. Tropea, editors. *Proceedings of 9th ERCOFTAC IAHR COST Workshop on refined turbulence modelling*, 2001.
6. R. Manceau and J.P. Bonnet, editors. *Proceedings of 10th ERCOFTAC IAHR QNET-CFD Workshop on refined turbulence modelling*, 2002.
7. S. Kapadia, S. Roy, and K. Wurtzler. Detached eddy simulation over a reference Ahmed car model. AIAA paper no. 2003-0857, 2003.
8. R.J.A. Howard and M. Pourquie. Large eddy simulation of an Ahmed reference model. *Journal of Turbulence*, 3, 2002.
9. M. Breuer and W. Rodi. Large eddy simulation of complex turbulent flows of practical interest. In E.H. Hirschel, editor, *Flow simulation with high performance computers II*, volume 52 of *Notes on Numerical Fluid Mechanics*, pages 258–274. Vieweg, Braunschweig, 1996.
10. C.M. Rhie and W.L. Chow. Numerical study of the turbulent flow past an airfoil with trailing edge separation. *AIAA Journal*, 21(11):1061–1068, 1983.
11. H. Werner and H. Wengle. Large-eddy simulation of turbulent flow over and around a cube in a plate channel. In *8th Symp. on Turb. Shear Flows*, 1993.